Rotational diffusion affects the dynamical self-assembly pathways of patchy particles

Newton, A.C.; Groenewold, J.; Kegel, W.K.; Bolhuis, P.G.

DOI
10.1073/pnas.1513210112

Publication date
2015

Document Version
Final published version

Published in
Proceedings of the National Academy of Sciences of the United States of America

Rotational diffusion affects the dynamical self-assembly pathways of patchy particles

Arthur C. Newton[a], Jan Groenewold[b], Willem K. Kegel[b], and Peter G. Bolhuis[a,1]

[a]Amsterdam Center for Multiscale Modeling, van 't Hoff Institute for Molecular Sciences, University of Amsterdam, 1090 GD Amsterdam, The Netherlands; and [b]van 't Hoff Laboratory for Physical and Colloid Chemistry, Debye Institute, Utrecht University, 3584 CH Utrecht, The Netherlands

Edited by William Bialek, Princeton University, Princeton, NJ, and approved November 4, 2015 (received for review July 6, 2015)

Predicting the self-assembly kinetics of particles with anisotropic interactions, such as colloidal patchy particles or proteins with multiple binding sites, is important for the design of novel high-tech materials, as well as for understanding biological systems, e.g., viruses or regulatory networks. Often stochastic in nature, such self-assembly processes are fundamentally governed by rotational and translational diffusion. Whereas the rotational diffusion constant of particles is usually considered to be coupled to the translational diffusion via the Stokes–Einstein relation, in the past decade it has become clear that they can be independently altered by molecular crowding agents or via external fields. Because virus capsids naturally assemble in crowded environments such as the cell cytoplasm but also in aqueous solution in vitro, it is important to investigate how varying the rotational diffusion with respect to transitional diffusion alters the kinetic pathways of self-assembly. Kinetic trapping in malformed or intermediate structures often impedes a direct simulation approach of a kinetic network by dramatically slowing down the relaxation to the designed ground state. However, using recently developed path-sampling techniques, we can sample and analyze the entire self-assembly kinetic network of simple patchy particle systems. For assembly of a designed cluster of patchy particles we find that changing the rotational diffusion does not change the equilibrium constants, but significantly affects the dynamical pathways, and enhances (suppresses) the overall relaxation process and the yield of the target structure, by avoiding (encountering) frustrated states. Besides insight, this finding provides a design principle for improved control of nanoparticle self-assembly.

kinetic networks | colloids | globular proteins | transition path sampling

In nature, self-assembled complex structures and networks often provide function. Prime examples are virus capsids, where capsomer proteins with specific interaction sites self-assemble into various structures, such as icosahedrons and dodecahedrons. Protein complexes can spontaneously form in the living cell, e.g., in signal transduction networks. Self-assembly of small designed building blocks can provide novel (bio)materials with desired properties. Such building blocks can consist of proteins, synthetic polypeptides, but also of colloidal particles. Particularly, the advent of novel synthesis routes for colloidal particles with a valence, so-called "patchy particles" opened up avenues for designing colloidal superstructures. Numerous experimental, theoretical, and numerical studies have enabled understanding of the phase behavior of these particles, predicting not only interesting building blocks for new functional materials, but also demonstrating new physics (1–5). Design principles for colloidal superstructures can predict which structure is the most thermodynamically favorable state (6). However, the fact that kinetics often trumps thermodynamics can hamper such design of colloidal superstructures. Strong directional binding and slow dissociation (7) can kinetically trap patchy-particle systems in a malformed state, rendering it unable to reach the designed equilibrium (ground) state. Controlling the self-assembly of colloidal particles thus requires understanding how the system evolves toward equilibrium, which is dictated by the kinetic network spanning all the states in which the system can occur. Several studies have demonstrated that the assembly toward the final ground state is affected by changing the interaction between patchy particles (8, 9), which affects both the thermodynamics and kinetics of the system. In contrast, here we study how the pathways change upon changing the dynamics only. Colloidal dynamics is often stochastic, and well described by overdamped Langevin (Brownian) dynamics (10). The rotational and translational diffusion constants of anisotropic particles are under standard conditions coupled via the Stokes–Einstein relation. However, in environments with high molecular crowding or in external fields the Stokes–Einstein relation is not necessarily valid anymore (11–13). Depending on the molecular crowder, the ratio between the rotational and translation diffusion constant can go up or down. Whereas crowding agents can in principle also change the binding equilibrium constants, this effect is expected to be weak if the specific interactions are sufficiently strong. Moreover, through the use of external fields, e.g., magnetic or electric, rotational motion could be controlled to a much further extent (14). In this work we investigate how varying the ratio of translational versus rotational diffusion constant influences the equilibrium kinetic network for small self-assembled clusters of colloidal patchy particles and how it could affect the design of self-assembling biological or artificial functional building blocks. Such particles provide a simple model for self-assembly of protein complexes such as in viruses or signal-transduction networks. Understanding and prediction of the colloidal self-assembly mechanisms requires the rates and pathways for all possible dissociation and association events in the kinetic network. However, on the timescale of the dynamics of the microscopic particles, binding and certainly dissociation processes are usually rare events due to high free-energy barriers caused by strong directional binding. As straightforward dynamical simulation

Significance

Recent experiments show that the rotational diffusion of proteins and patchy colloids does not always follow the Stokes–Einstein relation, especially in crowded environments or with the use of external fields. Because cellular cytoplasm is very crowded, this finding can have consequences for protein complex formation such as viruses. We study the kinetic network of simple models for proteins and patchy colloids and find that their dynamical self-assembly pathways change with varying the rotational diffusion constant. In particular, lowering the rotational diffusion avoids frustrated intermediate states. Such control of kinetic networks would also benefit the design of new self-assembled functional materials.

Author contributions: J.G., W.K.K., and P.G.B. designed research; A.C.N. and P.G.B. performed research; A.C.N. analyzed data; and A.C.N., W.K.K., and P.G.B. wrote the paper.

The authors declare no conflict of interest.

This article is a PNAS Direct Submission.

[1]To whom correspondence should be addressed. Email: p.g.bolhuis@uva.nl.

This article contains supporting information online at www.pnas.org/lookup/suppl/doi:10.1073/pnas.1513210112/-/DCSupplemental.

is extremely inefficient, we used the Single Replica Transition Interface Sampling (SRTIS) algorithm to collect all possible (un)binding trajectory ensembles relevant to the patchy colloid assembly (15).

Surprisingly, even for the dimerization of a one-patch particle we already find an effect of the rotation on the formation dynamics. Next, we investigate a dimerization of two-patch particles, which exhibits an intermediate state and multiple pathways of formation. However, the effect of the rotation becomes truly important if metastable intermediates are possible, such as in tetrahedron formation of a three-patch particle. Here we find that varying rotational diffusion favors one pathway over the other, without changing the equilibrium constants. Finally, we investigate the entire nine-state kinetic network of a tetrahedron cluster, and show that a change in the rotational diffusion shifts the preferred self-assembly pathways significantly. Whereas for low rotational diffusion the overall rate of tetrahedron formation decreases, frustrated states are avoided, leading to significantly less kinetic trapping.

In principle, this effect results in a better yield of the designed ground state, and in less kinetic trapping. Whereas in our examples the intermediate states are not truly kinetic traps, we envision that for more complex target structures, e.g., virus capsids, which compete against disordered aggregates, the price paid for slowing down the dynamics is outweighed by a preference for the correct self-assembly route and leads to higher relative yields. Experiments on protein complex formation and colloidal assembly should be able to test this prediction, for instance by searching for nonmonotonous behavior upon dilution of the crowding environment. Including the interplay between rotational and translational diffusion in the self-assembly design of new supracolloidal structures opens up new opportunities for improved control of bottom-up synthesis of functional materials. Controlling the dynamics could also lead to a design principle for functional materials where the target structure is not necessarily the thermodynamic ground state. Besides crowding agents, such control could be exerted on the rotational motion of the particles via external fields, such as in ref. 14. Moreover, this work helps in understanding how rotational diffusion influences self-assembly processes in naturally occurring crowded environments such as the cell. As it has been established that a crowded protein environment can decrease the ratio of rotational diffusion over the translation diffusion up to more than a factor of 3 (13), our simulations provide (an additional) explanation why protein complex assembly does not suffer more from kinetic trapping as one would naively expect.

Results and Discussion

Dimer of One-Patch Particles. Two hard spheres of radius σ with a single, relatively narrow, attractive patch (*Materials and Methods*), analogous to a binding site on a globular protein, can form a dimer. Although, due to the simplicity of the system, no energetically kinetic trap can exist, it is insightful to understand whether and how rotational diffusion can change the dynamical pathway taken during dissociation or association. We sample the path ensemble for this two-state binding process with SRTIS. The interfaces around stable states are defined by the energy of the system. We construct the free-energy landscape, as well as the (un)binding rate constants (*Materials and Methods*). Fig. 1 shows the free energy as a function of the distance between the particles, R_{12}, and the sum of the angles $\phi = \phi_1 + \phi_2$, with $\phi_{1,2}$ the angle between the patch vectors and the interparticle vector $\vec{R}_{12}$. The bound state (B) is the free-energy minimum at $\phi = 0$ and $R_{12} = \sigma$. At larger distances, the orientational part of the free energy becomes symmetric with respect to ϕ, indicating particles can freely rotate in the unbound state (U) where the interaction vanishes. Between these minima an (entropic) binding free-energy barrier is visible. Naturally, the free-energy landscape does not change with the rotational diffusion as it solely depends on the interactions between the particles. In contrast, varying the rotation diffusion ratio $f_{SE}^2 = D_r^0\sigma^2/3D_t^0$ significantly alters the dynamical pathways between B and U. Fig. 1 visualizes the projection of these dynamical paths, i.e., the reactive path density $n_r(\mathbf{q})$ (see *Materials and Methods* for a detailed definition) in the R_{12}, ϕ plane. The path density broadens for higher rotational diffusion, and significantly changes shape, as indicated by the red curve of maximum path density connecting U to B. Note that the path densities are the average of all reactive diffusive pathways (several individual trajectories are shown in the *SI Appendix*, section III). For fast rotational diffusion the path density at large distance becomes almost uniform. The observed enhancement at $\phi = \pi$ is due to the projection. The reactive path density also yields the orientational escape distribution as a function of ϕ at the boundary of the unbound state (Fig. 1). This distribution indicates the probability of dimer orientation at dissociation at $R_{12} = 2$, and is skewed to lower values of ϕ for low rotational diffusion, while becoming symmetric for high rotational diffusion. The change in reactive pathways is also visible in the reactive current (Fig. 1), which gives the average velocity at which the particles move along the reactive pathways, and hence does not contain off-pathway excursions. Both the reactive path density and the reactive current reveal that for low f_{SE}, i.e., slow rotational diffusion, the particles on average follow a straight pathway along the radial coordinate. For higher f_{SE}, and faster rotational diffusion, they follow a more curved association route from the unbound state into the attractive well. Note that due to microscopic reversibility, dissociation pathways are the reverse of the association trajectories. The difference in behavior can be understood by realizing that particles need to be aligned for binding. In the case of slow rotational diffusion, particles that are not aligned when close together will diffuse away transitionally before binding can occur.

The rate constants are given by $k_{IJ} = \phi_I P(\lambda_{0J}|\lambda_{1I}) = \phi_I P(\lambda_{mI}|\lambda_{1I}) P(\lambda_{0J}|\lambda_{mI})$, where ϕ_I is the flux out of state I, and $P(\lambda_{mI}|\lambda_{1I})$ and $P(\lambda_{0J}|\lambda_{mI})$ are crossing probabilities defined in *Materials and Methods*. The measured fluxes out of the stable states, the crossing probabilities and the rates are given in Table 1. Increasing rotational diffusion by 2 orders of magnitude enhances the absolute rates by a factor of 10. Nevertheless, the ratio between the rates does not change within the error bar, as this is determined by thermodynamics. Note that while the bond energy is $20k_BT$, the ratio $k_{BU}/k_{UB} \approx 0.1$, indicating that U is still relatively stable with respect to B. Of course, this is also dependent on the width of the attractive patch and the simulation volume (particle concentration).

Dimer of Two-Patch Particles. We subsequently performed SRTIS of dimer formation for particles with two patches, where association occurs via a multiple step mechanism. Fig. 2 shows the free energy and the reactive path density as a function of the bond distances $r_{1,2}$ (the bonds are identified in the bound state). This projection yields a more detailed assembly picture. Again, the free energy is independent of f_{SE} and shows a minimum at $r_1 = r_2 = 0$. Here the two particles do not concertedly assemble into the dimer state, but first form one bond, followed by a barrierless rotation around this bond into the dimer state. The two peaks near the dimer state around $r_{1,2} = 0.25\sigma$ in the reactive path density indicate both dimer permutations have been sampled. Note that the low path density at the origin is caused by the truncation of the paths as they reach the bound state. Increasing the rotational diffusion slightly changes the reactive path density toward a broader single-bond peak, as the requirement for alignment is relaxed, and hence concertedness decreases. To summarize, for fast rotational diffusion misalignment will still lead to binding, whereas less so for slow rotational diffusion.

Tetrahedron Assembly. To understand the effect of rotational diffusion on a more complex kinetic network, we study the formation of a tetrahedron consisting of particles with three patches. The patch vectors are set at an angle of 60° with respect to each other, so that the patches form an equilateral triangle on the surface of the

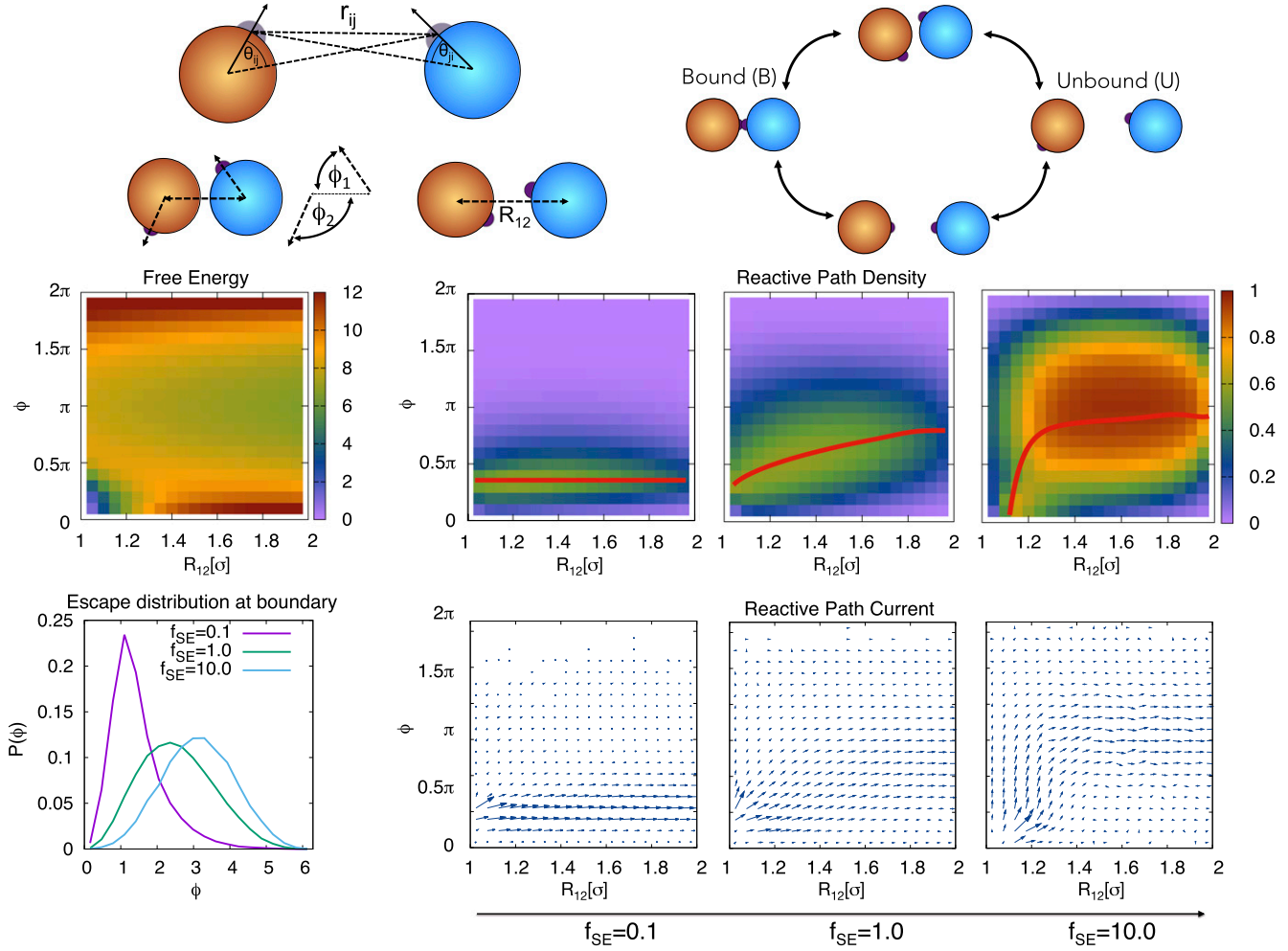

Fig. 1. (*Bottom*) Free energy, escape distributions, reactive path densities, and reactive currents for the one-patch particle system for different values of f_{SE} as a function of the distance between particles, R_{12}, and angle $\phi = \phi_1 + \phi_2$, with $\phi_{1,2}$ the angles between the patch vectors and the interparticle vector. (*Top*) Cartoon of dimer with parameters used in the potential, and order parameters used for the free energy and reactive path density plots. The binding pathway clearly changes with rotational diffusion constant, from more reactive pathways via translation for slow rotational diffusion toward reactive pathways more via rotation for fast rotational diffusion, without changing the free-energy landscape.

particle. The ground state of this system is a tetrahedron. As a first step, we study the final transition in the self-assembling process, namely the addition of the fourth particle to a preformed trimer cluster, while keeping the trimer constrained. Besides the bound state B and unbound state U, there is now also an intermediate state I where the fourth particle "wrongly" binds with two bonds to the trimer (Fig. 3, *Inset*). To escape from this frustrated intermediate state, a bond has to be broken before the complete tetrahedron can form. We study how the kinetic network between these three states changes when the rotational diffusion is varied. The rate calculation is more intricate than for the simple dimer system (*SI Appendix*, section I).

We performed SRTIS and computed the rate matrix $\mathbf{K}$ for different values of f_{SE}. The rate matrices are given in the *SI Appendix*, section IV, and can be used to compute the time evolution of the population by $\mathbf{p}(t) = \mathbf{p}(0)e^{-\mathbf{K}t}$. To show how f_{SE} influences the dissociation pathway we consider the ratio P_I/P_U of the intermediate state population over the unbound state. Fig. 3 shows this ratio as a function of time, for a system initially in the bound state. Whereas all curves decay eventually to the same equilibrium population, at short times the population ratio P_I/P_U scales roughly linear with the rotational diffusion ratio f_{SE}. Rotational diffusion thus significantly influences the pathways for self-assembly or disassembly.

Next, we examine the self-assembly of four free particles into a tetrahedron. We define a set of nine states: {Unbound state (U), one dimer (D_1), two dimers (D_2), trimer (Tr), frustrated trimer (Tr_f), frustrated tetramer states (T_{f1}, T_{f2}, T_{f3}) and the fully assembled tetrahedron state (T_d)} (see Fig. 4 for graphical representations). Again we do not define states that can transit to one of the nine defined states by barrierless rotation around bonds. Performing an SRTIS simulation results in a complete rate matrix $\mathbf{K}$ (given in *SI Appendix*, section IV). Applying transition path theory (TPT) to these rate matrices results in flux matrices, as well as committors for each state for the transition from U to T_d (16, 17) (see *SI Appendix*, section I for details). Fig. 4 shows a graphical summary of this information for different values of f_{SE}. Whereas the net flux generally decreases with decreasing rotational diffusion, the thickness of arrows corresponds to the normalized net flux, to emphasize the differences in topology. For slow rotational diffusion $f_{SE} = 0.1$, the $U - D - T_r - T_d$ pathway carries most of the flux. For higher f_{SE}, the T_r state is avoided, as was the case in the constrained tetrahedron system. Indeed, at high rotational diffusion, the transition between U and T_d occurs preferably via frustrated states, T_{f1}, T_{f2}, and T_{f3}, which are then more accessible. Transitions along Tr_f are favorable, even for low f_{SE}, probably due to

Table 1. Flux, crossing probabilities, and rates from TIS for one patch dimer assembly with f_{SE} = 0.1, 1.0, and 10.0 in MC cycle units; subscript denotes error in last digit

f_{SE}	State	$\langle\phi_{0I}\rangle$	$P(\lambda_{mI}\|\lambda_{1I})$	$P(\lambda_{0J}\|\lambda_{mI})$	k_{IJ}
0.1	B	$3.58_4\times10^{-3}$	4.03×10^{-5}	0.223_9	$3.3_1\times10^{-8}$
	U	$1.29_1\times10^{-3}$	3.58×10^{-2}	0.0059_1	$3.0_1\times10^{-7}$
1.0	B	$5.22_4\times10^{-3}$	8.86×10^{-5}	0.216_1	$1.00_1\times10^{-7}$
	U	$1.312_9\times10^{-3}$	4.52×10^{-2}	0.015_3	$9.4_1\times10^{-7}$
10.0	B	$1.669_1\times10^{-2}$	1.51×10^{-4}	0.043_3	$5.06_7\times10^{-7}$
	U	$1.47_2\times10^{-3}$	5.10×10^{-2}	0.039_3	$5.05_9\times10^{-6}$

combinatorial entropy because there are more ways to (dis)assemble into Tr_f than into Tr. Another way to demonstrate the influence of rotational diffusion on the assembly is to show the population dynamics of the trimer state, Tr, over the frustrated tetramer state, T_{f2} (Fig. 4). The population of the trapped intermediate state T_{f2} is initially significantly less populated for slow than for fast rotational diffusion, indicating that indeed for assembly with fast rotational diffusion particles aggregate more easily toward frustrated states. Indeed, this also implies that for larger systems beyond the tetramer the frustrated states will lead to an even stronger trapping effect. In the *SI Appendix*, section V we show that the correctly formed tetrahedron pathway dominates for slow rotational diffusion by analyzing the rate matrices using such strong traps.

In Fig. 4 the committor q_i^+, defined as the probability that from state i state T_d will be reached before reaching U, is shown as function of f_{SE}. The committor for the frustrated tetramers decreases with decreasing f_{SE}. In contrast, the probability for Tr increases, indicating again that for slow rotational diffusion a less frustrated pathway is followed.

We note that the overall process always becomes slower when decreasing rotational diffusion, even when scaled with the dwell time in the unbound state (*SI Appendix*, section V). However, instead of keeping the translational diffusion fixed and varying the rotational diffusion constant, we can view our results in terms of a fixed rotational diffusion constant and a varying translational diffusion. Then the timescale for tetrahedron formation becomes shorter for lower rotational diffusion.

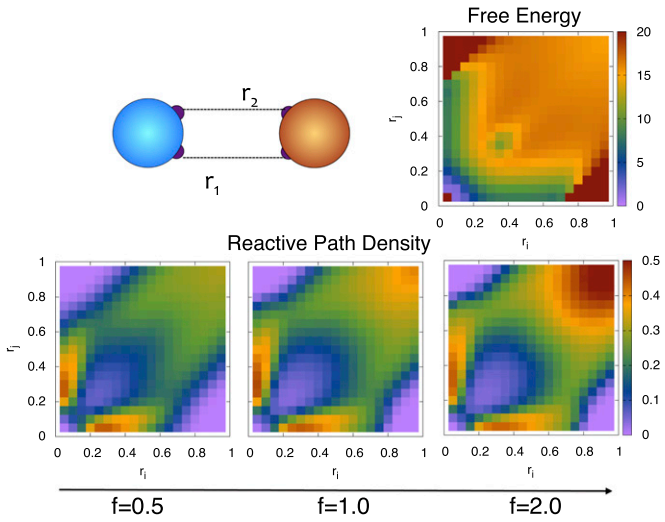

Fig. 2. Free energy and reactive path densities for the two-patch particle system for different values of f_{SE} as a function of the distance $r_{i,j}$ between the formed bonds in the bound state. The concertedness of assembly is changed by changing the rotational diffusion. For fast rotational diffusion misalignment will still lead to binding, whereas less so for slow rotational diffusion.

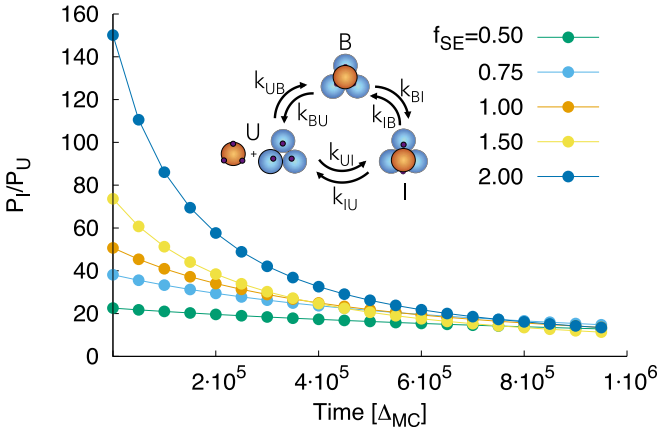

Fig. 3. Population ratio for the intermediate state over the unbound state, as the system relaxes starting from a fully populated bound state, for different rotational diffusion constants. For fast rotational diffusion, the intermediate state is relatively more populated than for slow rotational diffusion. For all rotational diffusion constants the system equilibrates toward the same thermodynamic state.

Summary

Our path-sampling simulations demonstrate the proof-of-concept that altering the rotational diffusion can affect the kinetic network and hence the mechanism of self-assembly for simple patchy-particle systems. For the dimer system of one-patch and two-patch particles the mechanism of reactive pathways changes significantly with rotational diffusion, from a translational reactive pathway for slow rotational diffusion, to a rotational reactive pathway for fast rotational diffusion. The pathways do not need to follow the free-energy landscape, and avoid the saddle point when the dynamics are changed. In the assembly of a constraint tetrahedron of four particles decorated with three patches, faster rotational diffusion increases the likelihood of a route via the intermediate state. This effect is even stronger for the full tetrahedron assembly, where the frustrated states and kinetic traps are avoided when rotational diffusion is suppressed. We argue that these results hold beyond the tetramer, and can be seen as a generic effect governed by the different roles that rotation and translation play in the self-assembly. Whereas translational motion is important in particle binding, rotation is crucial for transitions between misaligned frustrated states. We support this argument by analyzing the population dynamics of a simple Markov model that mimics a much larger assembly process (*SI Appendix*, section VI). This analysis clearly shows that slower rotational diffusion results in less frustration and in orders of magnitude higher yields, and generalizes our finding into a genuine principle for controlling and understanding complex self-assembly kinetics.

Materials and Methods

Model. We model the particles as patchy hard spheres with diameter σ. For a center-to-center distance, $\sigma < R_{ij} < 2\sigma$, the patch potential is:

$$u_{ij}(\mathbf{R}_{ij},\mathbf{\Omega}) = -\epsilon \sum_{p_{ij}} e^{-kr_{ij}}\, e^{-\left(\theta_i^2+\theta_j^2\right)/w^2}, \qquad [1]$$

where $\mathbf{\Omega}$ denotes the orientation of the particles, the sum is over all patch pairs p_{ij}, k controls the range of the interaction, r_{ij} is the distance between patch centers, θ_α is the angle between the patch vector of particle α and the vector connecting the center of α and the center of the patch on the other particle, and w is a parameter that controls the patch width (Fig. 1). Note that the arccosine is needed for the angle calculation. As the patch widths in this work are all small, we approximated the arccosine to speed up the simulation significantly.

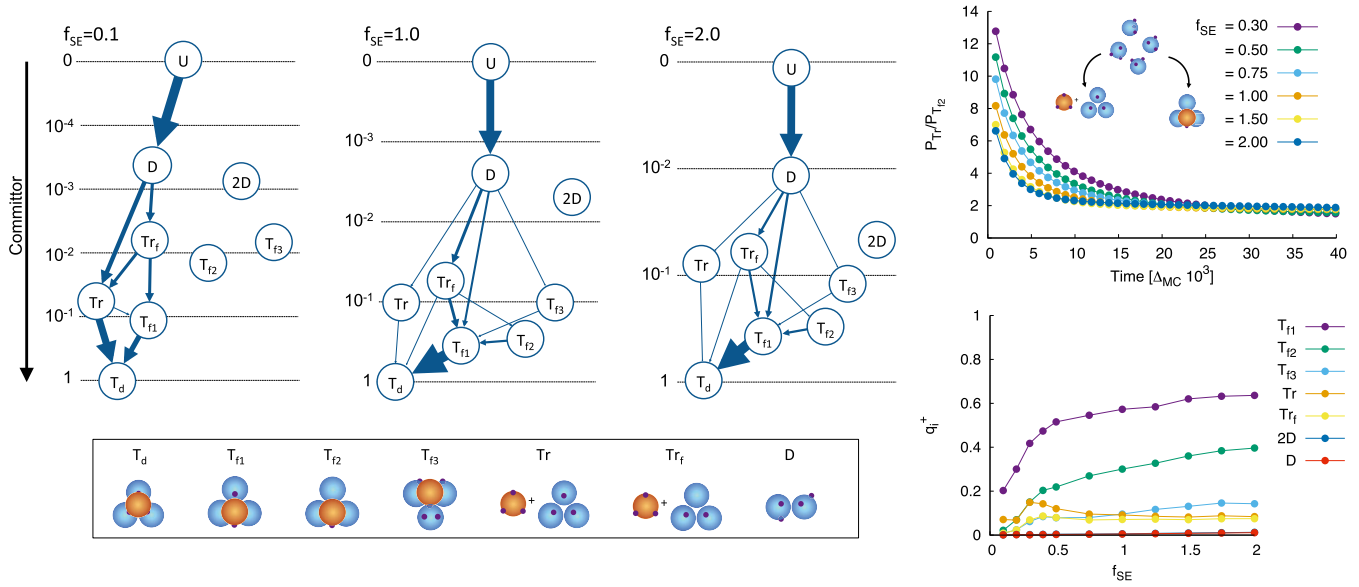

Fig. 4. (*Bottom*) Cartoon images of all states defined except for the unbound state. (*Top Left*) Net flux graph for the tetrahedron assembly. The arrow size indicates the relative magnitude of the flux. For faster rotational diffusion, the system avoids the trimer state *Tr* more than for slow diffusion, and follows a more frustrated pathway via states T_{f1}, T_{f2}, and T_{f3}, an extension of the principle shown for the constrained tetrahedron system. (*Top Right*) Population ratio for the trimer state, *Tr*, over the frustrated tetramer state, T_{f2}, as the system relaxes starting from a fully unbound state for different rotational diffusion constants, demonstrating how the system equilibrates during assembly. For fast rotational diffusion the trimer state is more populated during the equilibration. For all rotational diffusion constants the system equilibrates toward the same thermodynamic state. (*Bottom Right*) Committors to T_d, q_i^+, for all intermediate states as a function of the rotational diffusion factor, f_{SE}. The committor for the frustrated tetramers decreases with decreasing f_{SE}. In contrast, the committor for *Tr* (relatively) increases.

Dynamic Monte Carlo. In our simulations we used dynamic Monte Carlo (DMC) to evolve the system in time via translational and rotational MC moves. A translation move displaces a randomly chosen particle by a random amount in the interval $[-\delta_t, \delta_t]$ and a rotation move rotates a randomly chosen particle over an angle randomly chosen between [0, δ_r]. The rotational diffusion constant can effectively be varied relative to the translational diffusion constant, by changing the maximum rotational step size, δ_r, relative to the maximum translational step size, δ_t (18). This amounts to changing the factor f_{SE} in the generalized Stokes–Einstein relation $D_r^0 = 3f_{SE}^2 D_t^0 \sigma^{-2}$. The advantage of this approach with respect to a more complicated rotational Brownian dynamics approach is its simplicity, and its very effective control over the rotational diffusion. We stress that a full rotational Brownian dynamics approach will not qualitatively alter the results. The DMC simulations consist of one MC cycle per frame, where each MC cycle consists of *N* translational and rotational MC moves, where *N* is the number of particles. The maximum translational displacement is set to 0.005σ for all cases except the full tetrahedron, where, due to long diffusive paths, we set the translational step to 0.02σ to decrease path lengths. Taking a colloidal suspension in water, with colloids with a size of 1 μm, and using the Stokes–Einstein relation to compute the translational diffusion, $D_t^0 = k_B T/(3\pi\eta\sigma)$, we can estimate the actual time step via $\Delta t = (\delta_t/\sigma)^2 \bar{a}_t/(6D_t^0)$, so every MC cycle corresponds roughly to 7 μs. For proteins, which are roughly 100× smaller, this time becomes $\sim 10^2$ ns. The rotational step size is multiplied with f_{SE}, which changes the rotational diffusion quadratically. The average acceptance ratios $\bar{a}_t$ and $\bar{a}_r$ are always higher than 0.7. It has been demonstrated that this regime leads to proper diffusive dynamics (18, 19).

SRTIS. SRTIS requires a set *S* of chosen stable states and predefined interfaces around these stable states. The method samples unbiased dynamical trajectories that leave a particular state by the traditional path sampling shooting move, but in addition imposes a bias that enhances crossing of the interfaces via a Wang–Landau scheme. Special moves for switching between stable states enable efficient sampling of all allowed path ensembles in the entire kinetic network. From these ensembles we can subsequently calculate the free energy of the system, get mechanistic insight, and calculate the entire rate network (15, 20, 21).

Simulation Settings.

One-patch dimer. Two hard spheres of radius σ are each decorated with one patch of range $k^{-1} = 4.0\sigma$ and width $w = 0.7$. Note that for this value of *w*, the potential depth $\epsilon = 20k_BT$ has to be sufficiently high for a stable dimer. The dimer is put in a periodic cubic box of size 5σ, which sufficiently stabilizes the unbound state. Only two different states are defined, the bound state (*B*), when the energy of the system, $E_{sys} = \sum_{i<j} u_{ij}$, is lower than $-12k_BT$, and the unbound state (*U*), when the particles are separated more than 2σ, which is also where we truncate the potential to zero. For the bound state we choose the first interface at the stable state definition and the rest of the interfaces are separated by $3k_BT$ until maximum energy is reached. The unbound state requires many interfaces close to the zero-point energy: $\{0, 0, 10^{-14}, 10^{-12}, 10^{-10}, 10^{-8}, 10^{-6}, 10^{-4}, 10^{-2}\}$, to bias the system toward *B* also when the particles are not properly aligned.

Two-patch dimer. The potential parameters are identical to one patch case, except that the patch width is decreased ($w = 0.01$) to ensure the two patches do not overlap. The state and interface definition are identical to the one-path system, except more interfaces surround the bound state, because the bound state is lower in energy.

Tetramer. Model parameters for this system are $\epsilon = 12k_BT$, $w = 0.01$, and $k = 4.0\sigma^{-1}$. To decrease the diffusive pathway for the four particles, we altered the box size for this system to 4.0σ. The bound state is defined as $E_{sys} < -20k_BT$, with three correct bonds formed, and the intermediate state as $E_{sys} < -10k_BT$, with two bonds formed in a frustrated state. Again, we use the system energy as the order parameter for the interfaces. The interfaces for each state are separated by $3k_BT$ starting from their minimum energy. The same interfaces and state definition for the unbound state as before are used. Each state is recognized according to their appropriate topology defined by their bonds.

Rates. The rate of the system can be obtained via (22)

$$k_{IJ} = \phi_I P(\lambda_{0J}|\lambda_{1I}), \qquad [2]$$

where ϕ_I is the flux out of the stable state *I* and $P(\lambda_{0J}|\lambda_{1I})$ is the crossing probability from the first interface of state *I* to the first interface of state *J*, which can be factorized into the crossing probability $P(\lambda_{ml}|\lambda_{1I})$ and $P(\lambda_{0J}|\lambda_{ml})$. The flux is easily calculated with a standard DMC run, or from the minus interface ensemble (22–24). The crossing probabilities are usually very small and therefore difficult to obtain. However, because SRTIS biases the paths to cross the barrier, we can obtain good statistics on the crossing probability by performing the weighted histogram analysis method (WHAM) on the crossing probabilities for every interface. For more details, see *SI Appendix*, section I.

Free Energy from the Path Ensemble. We collect the full path ensemble for dimerization via SRTIS and from this ensemble we can calculate the free-energy landscape (21):

$$F(\mathbf{q}) = -k_B T \log p(\mathbf{q}) + C$$
$$p(\mathbf{q}) = C \int \mathcal{D}\mathbf{x}^L \mathcal{P}_c[\mathbf{x}^L] \sum_{k=0}^{L} \delta[\mathbf{q}(\mathbf{x}_k) - \mathbf{q}], \quad [3]$$

where C is an arbitrary constant, $\int \mathcal{D}\mathbf{x}^L$ is the integral over the ensemble of pathways $\mathbf{x}^L$ consisting of L time frames $\mathbf{x}_k$, $\mathbf{q}(\mathbf{x}_k)$ are the collective variables at time frame $\mathbf{x}_k$, and $\mathcal{P}_c[\mathbf{x}^L]$ is the path probability. In SRTIS we obtain the Wang–Landau biased path ensemble. To reweight the path ensemble, we use the crossing probabilities obtained from WHAM. Therefore, the path probability in Eq. **3** is the reweighted path ensemble with weights $\overline{w}_j^i = (\sum_{j=1}^{i} 1/w_j^i)^{-1}$, where w_j^i are the optimized WHAM weights for each interface histogram. The reweighted path probability then becomes (21)

$$\mathcal{P}_c[\mathbf{x}^L] = \sum_{I \in S} c_I \left[w_1^I P_{\Lambda_1}^-[\mathbf{x}^L] + \sum_{j=1}^{n-1} \mathcal{P}_{I\Lambda_j}[\mathbf{x}^L] W^I[\mathbf{x}^L] \right], \quad [4]$$

where $\mathcal{P}_{I\Lambda_j}$ and $P_{\Lambda_1}^-$ denote the path probability for interface j of state I and the minus interface, respectively. The constants c_I are obtained via matching the rates from all states, and $W^I[\mathbf{x}^L] = \sum_{i=1}^{n-1} \overline{w}_i^I g_i^I[\mathbf{x}^L]$, where $g_i^I[\mathbf{x}^L] = \theta(\lambda_{max}[\mathbf{x}^L] - \lambda_i)\theta(\lambda_{i+1} - \lambda_{max}[\mathbf{x}^L])$ selects the correct weight $\overline{w}_i^I$ for a path that has its maximum λ between interface i and $i+1$. One could histogram all of the free energies after the simulation using saved pathways after one has obtained the proper weights. However, as every path that has reached a certain maximum interface based on λ_{max} is reweighted with the same weight, it is better to histogram on the fly for each interface separately, and subsequently reweight and sum all of the histograms. As such, no paths need to be stored for subsequent analysis.

Reactive Path Density. The reactive path density is defined as

$$n_r(\mathbf{q}) = \int \mathcal{D}\mathbf{x}^L \mathcal{P}_r[\mathbf{x}^L] h_{\mathbf{q}}(\mathbf{x}^L) \sum_{k=0}^{L} \delta[\mathbf{q}(\mathbf{x}_k) - \mathbf{q}]. \quad [5]$$

The function $h_{\mathbf{q}}(\mathbf{x}^L)$ is 1 if the path has not visited $\mathbf{q}(\mathbf{x}_k)$ the before kth time step, and zero otherwise; $\mathcal{P}_r[\mathbf{x}^L]$ is the reactive path probability given by $\mathcal{P}_c[\mathbf{x}^L] h_A(\mathbf{x}_0) h_B(\mathbf{x}_L)$, where h_A and h_B ensures that only reactive pathways are taken into account. Note that a path density does not add up to unity.

Reactive Path Current. The reactive path current is (17)

$$J_{BU}(\mathbf{q}) = C \int \mathcal{D}\mathbf{x}^L \mathcal{P}_r[\mathbf{x}^L] \sum_{k=0}^{L} \delta[\mathbf{q}(\mathbf{x}_k) - \mathbf{q}] \dot{q}(\mathbf{x}_k), \quad [6]$$

where $\dot{q}(\mathbf{x}_k)$ is the estimated velocity in the projected space $\mathbf{q}$. This current has the same properties as the reactive path density, except for the fact that dead ends are averaged out, which results in the mean direction a path will follow.

Nested States and Flux Analysis. Details on the rate calculation for nested states and the flux analysis using TPT are given in the *SI Appendix*, section I.

ACKNOWLEDGMENTS. This work is part of the research program of the Foundation for Fundamental Research on Matter (FOM), which is part of the Netherlands Organisation for Scientific Research (NWO).

1. Glotzer SC, Solomon MJ (2007) Anisotropy of building blocks and their assembly into complex structures. *Nat Mater* 6(8):557–562.
2. Martinez-Veracoechea FJ, Mladek BM, Tkachenko AV, Frenkel D (2011) Design rule for colloidal crystals of DNA-functionalized particles. *Phys Rev Lett* 107(4):045902.
3. Chen Q, Bae SC, Granick S (2011) Directed self-assembly of a colloidal kagome lattice. *Nature* 469(7330):381–384.
4. Smallenburg F, Sciortino F (2013) Liquids more stable than crystals in particles with limited valence and flexible bonds. *Nat Phys* 9(9):554–558.
5. Smallenburg F, Filion L, Sciortino F (2014) Erasing no-man's land by thermodynamically stabilizing the liquid-liquid transition in tetrahedral particles. *Nat Phys* 10(9):653–657.
6. Preisler Z, Vissers T, Munaò G, Smallenburg F, Sciortino F (2014) Equilibrium phases of one-patch colloids with short-range attractions. *Soft Matter* 10(28):5121–5128.
7. Kraft DJ, et al. (2012) Surface roughness directed self-assembly of patchy particles into colloidal micelles. *Proc Natl Acad Sci USA* 109(27):10787–10792.
8. Hagan MF, Chandler D (2006) Dynamic pathways for viral capsid assembly. *Biophys J* 91(1):42–54.
9. Klein HC, Schwarz US (2014) Studying protein assembly with reversible Brownian dynamics of patchy particles. *J Chem Phys* 140(18):184112.
10. Northrup SH, Erickson HP (1992) Kinetics of protein-protein association explained by Brownian dynamics computer simulation. *Proc Natl Acad Sci USA* 89(8):3338–3342.
11. Kuttner YY, Kozer N, Segal E, Schreiber G, Haran G (2005) Separating the contribution of translational and rotational diffusion to protein association. *J Am Chem Soc* 127(43):15138–15144.
12. Li C, Wang Y, Pielak GJ (2009) Translational and rotational diffusion of a small globular protein under crowded conditions. *J Phys Chem B* 113(40):13390–13392.
13. Wang Y, Li C, Pielak GJ (2010) Effects of proteins on protein diffusion. *J Am Chem Soc* 132(27):9392–9397.
14. Yan J, Bloom M, Bae SC, Luijten E, Granick S (2012) Linking synchronization to self-assembly using magnetic Janus colloids. *Nature* 491(7425):578–581.
15. Du WN, Bolhuis PG (2013) Adaptive single replica multiple state transition interface sampling. *J Chem Phys* 139(4):044105.
16. Noé F, Schütte C, Vanden-Eijnden E, Reich L, Weikl TR (2009) Constructing the equilibrium ensemble of folding pathways from short off-equilibrium simulations. *Proc Natl Acad Sci USA* 106(45):19011–19016.
17. E W, Vanden-Eijnden E (2010) Transition-path theory and path-finding algorithms for the study of rare events. *Annu Rev Phys Chem* 61(1):391–420.
18. Romano F, De Michele C, Marenduzzo D, Sanz E (2011) Monte Carlo and event-driven dynamics of Brownian particles with orientational degrees of freedom. *J Chem Phys* 135(12):124106.
19. Williamson AJ, Wilber AW, Doye JP, Louis AA (2011) Templated self-assembly of patchy particles. *Soft Matter* 7(7):3423–3431.
20. Du W, Bolhuis PG (2014) Sampling the equilibrium kinetic network of Trp-cage in explicit solvent. *J Chem Phys* 140(19):195102.
21. Rogal J, Lechner W, Juraszek J, Ensing B, Bolhuis PG (2010) The reweighted path ensemble. *J Chem Phys* 133(17):174109.
22. van Erp TS, Moroni D, Bolhuis PG (2003) A novel path sampling method for the calculation of rate constants. *J Chem Phys* 118(17):7762–7774.
23. Van Erp TS, Bolhuis PG (2005) Elaborating transition interface sampling methods. *J Comput Phys* 205(1):157–181.
24. Swenson DW, Bolhuis PG (2014) A replica exchange transition interface sampling method with multiple interface sets for investigating networks of rare events. *J Chem Phys* 141(4):044101.